Journal of Hydroscience and Hydraulic Engineering
Vol.21, No.1 May, 2003, 1-10

DIRECT NUMERICAL SIMULATION OF COHERENT VORTEX STRUCTURES IN AN OPEN-CHANNEL FLOW OVER DUNE TYPE WAVY BED

By

Shun-ichiro Hayashi

Section Manager, Department of Civil Engineering, Kumamoto Prefectural Government,
6-18-1 Suizenji, Kumamoto, Japan

Terunori Ohmoto

Associate Professor, Department of Civil and Environmental Engineering,
Kumamoto University, 2-39-1 Kurokami, Kumamoto, Japan

and

Kiyoshi Takikawa

Professor, Research and Education Center of Coastal Environmental Science,
Kumamoto University, 2-39-1 Kurokami, Kumamoto, Japan

SYNOPSIS

In this study, a fully-developed three-dimensional turbulent flow over a plural solid dune bed in an open-channel was reproduced by direct numerical simulation (DNS). Its coherent structures were also examined by using time-line technique and an identification of cylindrical vortex tubes. "Boil of the first kind", which was unique to the flow field on dune-type sand waves, was numerically reproduced. It was found that the kolk which causes the boil of the first kind can be detected as cylindrical vortex tubes rising from the bed. Findings also show that the boil of first kind and the kolk were generated not only from "hairpin vortices" as previously noted, but also from "reverse hairpin vortices" with their head near the bed and cyclonic vortices at their foot.

INTRODUCTION

Mechanisms of sand wave generation and turbulent structures are very interesting matters in view of flood control. While these matters have long been addressed by numerous researchers and engineers through various observations and experiments, there are still a number of unsolved problems regarding large vortex structures such as circular boils that intermittently occur on river surfaces. In the past, Matthes [10] assumed that boils were generated by whirlwind-type upward vortices extending from the riverbed to the surface and defined this upward vortex as a kolk vortex. Jackson [7] inferred that boils are caused by bursts based on the observation that boils tend to be generated at sand wave valleys at frequencies nearly equal to that of burst frequencies. Boils found in straight river channels are now classified into three kinds based on their generation mechanisms [11]. While boils of the third kind, which are caused by bursting, are generated regardless of the shape of riverbed, boils of the first and second kinds are thought to be caused by sand waves in

the streamwise and span directions, respectively. Because boils of the third kind usually occur less frequently in high-Reynolds-number flows such as rivers, boils associated with dune-type sand waves are expected to be boils of the first kind, caused mainly by kolk vortices. Nezu and Nakagawa [12] and Nezu [14] made observations and time-space correlation analyses by using Laser-Doppler anemometry and the hydrogen bubble method, and argued, based on cross-sectional and three-dimensional properties, that systematic vortices generated behind continuous sand waves could be explained by a horseshoe-shaped vortex model. It is expected that detailed coherent structures will reveal in the future with the advancement of image processing techniques such as PIV and PTV.

Coherent structures of turbulence can be clarified with the aid of dramatic advancements in computers and computational fluid dynamics (CFD). In particular, DNS and LES deepen our knowledge about turbulence by providing information on instantaneous three-dimensional coherent turbulence structures [1]. While conventional hydrogen bubble and dye injection methods can only visualize segmental coherent structures indirectly, CFD allows us to directly identify of vortex structures over time and space by using various detecting parameters as well as pressure. Therefore, a better explanation of the results of flow visualization can be achieved by correlating coherent structures to the results of conventional visualization methods in addition to making detailed discussions on vortex structures.

In the present study, DNS is applied to open-channel turbulence fields that have dune-type fixed sand waves in order to investigate the generation mechanism of large vortices by directly identifying their coherent structures and by examining the correlation between kolk vortices and boils of the first kind.

NUMERICAL ANALYSIS METHOD

Subject of analysis and calculation method

The turbulence field of a fully developed straight open channel which has dune-type continuous fixed waves was analyzed. The bottom shape and the bed height of the channel were set as shown in Figure 1 after the method of Nezu et al [15]. Sidewall effects were eliminated from the flow field by providing periodic boundary conditions in the streamwise and span directions.

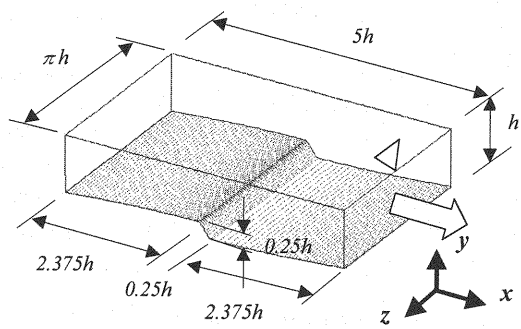

Fig. 1 Computational Domain

To enable compatibility with arbitrary boundaries, Navier-Stokes and pressure-Poisson equations mapped to a three-dimensional general coordinate system were used as the basic equations (equations (1) and (2)). The boundary conditions consisted of non-slip velocity at the bottom, slip velocity for u and w at the free surface, and Neumann pressure conditions are applied. A grid of $96 \times 65 \times 64$ was generated by using the method of Steger and Sorenson [16]. The Reynolds number of 3300 was adopted based on the average velocity and the average water depth. The other algorithms adopted here are the same as reported previously [2,3,4].

$$\frac{\partial u_i}{\partial t}+u_j\frac{\partial \xi_k}{\partial x_j}\frac{\partial u_i}{\partial \xi_k}=-\frac{\partial \xi_j}{\partial x_i}\frac{\partial p}{\partial \xi_j}+\frac{1}{\mathrm{Re}}\left(\frac{\partial \xi_j}{\partial x_l}\frac{\partial \xi_k}{\partial x_l}\frac{\partial^2}{\partial \xi_j\partial \xi_k}+\frac{\partial^2}{\partial x_l\partial x_l}\frac{\partial}{\partial \xi_j}\right)u_i \tag{1}$$

$$\begin{aligned}\left(\frac{\partial \xi_j}{\partial x_i}\frac{\partial \xi_k}{\partial x_i}\frac{\partial^2}{\partial \xi_j\partial \xi_k}+\frac{\partial^2 \xi}{\partial x_i\partial x_i}\frac{\partial}{\partial \xi_j}\right)p=&\frac{1}{\Delta t}\left(\frac{\partial \xi_j}{\partial x_i}\frac{\partial u_i}{\partial \xi_j}\right)-\frac{\partial \xi_k}{\partial x_i}\frac{\partial \xi_l}{\partial x_j}\frac{\partial u_j}{\partial \xi_k}\frac{\partial u_i}{\partial \xi_l}\\&+u_j\frac{\partial \xi_k}{\partial x_j}\frac{\partial}{\partial \xi_k}\left(\frac{\partial \xi_l}{\partial x_i}\frac{\partial u_i}{\partial \xi_l}\right)\\&+\frac{1}{\mathrm{Re}}\left(\frac{\partial \xi_j}{\partial x_i}\frac{\partial \xi_k}{\partial x_i}\frac{\partial^2}{\partial \xi_j\partial \xi_k}+\frac{\partial^2 \xi_j}{\partial x_i\partial x_i}\frac{\partial}{\partial \xi_j}\right)\left(\frac{\partial \xi_m}{\partial x_l}\frac{\partial u_i}{\partial \xi_m}\right)\end{aligned} \tag{2}$$

Computational results

Figures 2 and 3 show a vertical distribution and contours of mainstream velocity $U^+ \equiv U/U_\tau$. The superscript "+" indicates an inner-layer physical quantity. The figures indicate the occurrence of boundary-layer separation behind the crest, the presence of a back-flow area and a reattachment point. The ratio of reattachment-point distance to the wave height is about 4.8, which agrees with the results of continuous sand wave experiments carried out by Nezu et al [13]. Figure 4 shows a spatial distribution of Reynolds stresses, $-\overline{u^+v^+}$. As is the case with experimental results[13], there is a continuous peak area along the inflection points extending from the crest to the reattachment point. The maximum stress value occurs at a location above the reattachment point, indicating generation of a strong Reynolds stress caused by the collision of the separation vortex to the bed.

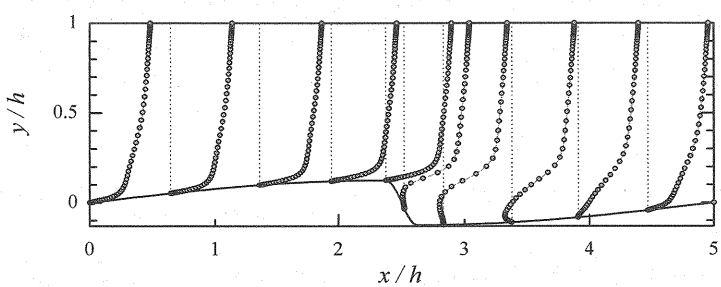

Fig. 2 Distribution of mainstream velocity U^+

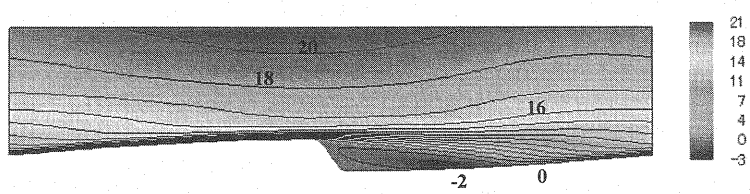

Fig. 3 Contour lines of mainstream velocity U^+

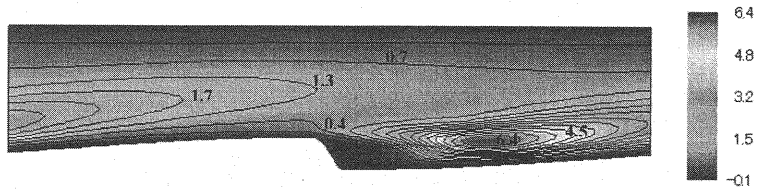

Fig. 4 Contour lines of Reynolds shear stress $-\overline{u^+v^+}$

VISUALIZATION OF COHERENT STRUCTURES

Time-lines

The time-line method can be used to visualize coherent structures. Two hundred tracer sources were arranged in the horizontal direction near the surface ($y/h = 0.95$) and the marker particles were generated at regular intervals ($\Delta t^+ = 0.6$) to obtain the results shown in Figure 5. While no low- and high-speed streaks were observed near the free surface, an elliptical blank area with a diameter comparable to the water depth occurred. This is considered to be a splat. Splattings are at the center of the diverged velocity vectors with a positively vertical velocity fluctuation on the free surface, caused by upwelling that is characteristic of open-channel turbulence. Because a splat was not observed in the time-line analysis of a flat open channel, the observed splat was thought to be a boil. Figure 6 shows time-line diagrams of a vertical cross-section passing the center of the splat ($z/h = 1.25$). Because of the acceleration and deceleration associated with the shape of the bed, the flows in the diagrams are much more disturbed and complicated than those over flat beds. There is a large spiral vortex inclining streamwise and extending from the bed to the splat. This is a kolk vortex that swirls up riverbed material, and the splat is considered to be a boil of the first kind. However, the question remains, whether coherent vortices can be identified correctly in real time because flow hysteresis is overlapped in the time-line diagrams.

Rotating tubular vortices (low-pressure vortices)

Methods of visualizing coherent structures directly have recently been proposed, and their generation mechanisms and detailed properties are examined carefully [6, 8]. The Q definition method [6] described below, is used in the present study.

When this method is used, a vortex is defined by the area where the second invariant Q of the velocity gradient tensor ∇u, is positive. This is based on the fact that the Q value expressed as equation (3) is positive when the vorticity exceeds the shear strain.

$$Q \equiv \frac{1}{2}\left[\left(\frac{\partial u_i}{\partial x_i}\right)^2 - \frac{\partial u_i}{\partial x_j}\frac{\partial u_j}{\partial x_i}\right] = -\frac{1}{2}\frac{\partial u_i}{\partial x_j}\frac{\partial u_j}{\partial x_i} = \frac{1}{2}\left(\|\Omega\|^2 - \|S\|^2\right) \tag{3}$$

where $S_{ij} = \frac{1}{2}\left(\frac{\partial u_i}{\partial x_j} + \frac{\partial u_j}{\partial x_i}\right)$, $\Omega_{ij} = \frac{1}{2}\left(\frac{\partial u_i}{\partial x_j} - \frac{\partial u_j}{\partial x_i}\right)$

Because this condition corresponds to the source term of the pressure Poisson equation ($\nabla^2 p = 2\rho Q$), the area of $Q>0$ means a local low-pressure area containing a minimum pressure value and a higher Q value means a stronger vortex. Therefore, the Q definition method coincides with the definition method based on a positive pressure Laplacian [14] and yields almost the same results as the λ_2-definition method [8].

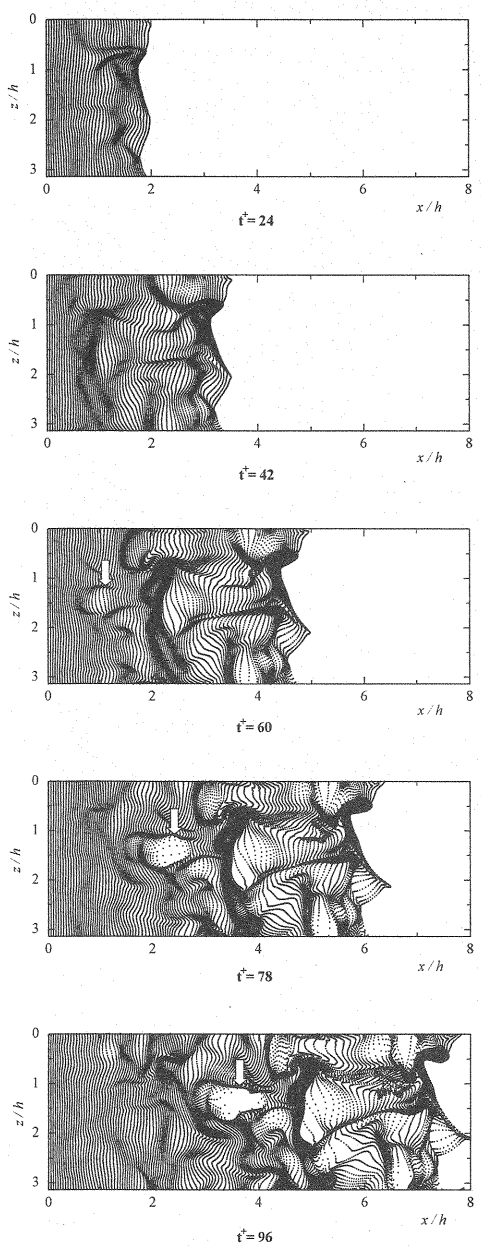

Fig. 5 Time-line diagrams for a horizontal plane (y/h=0.95)

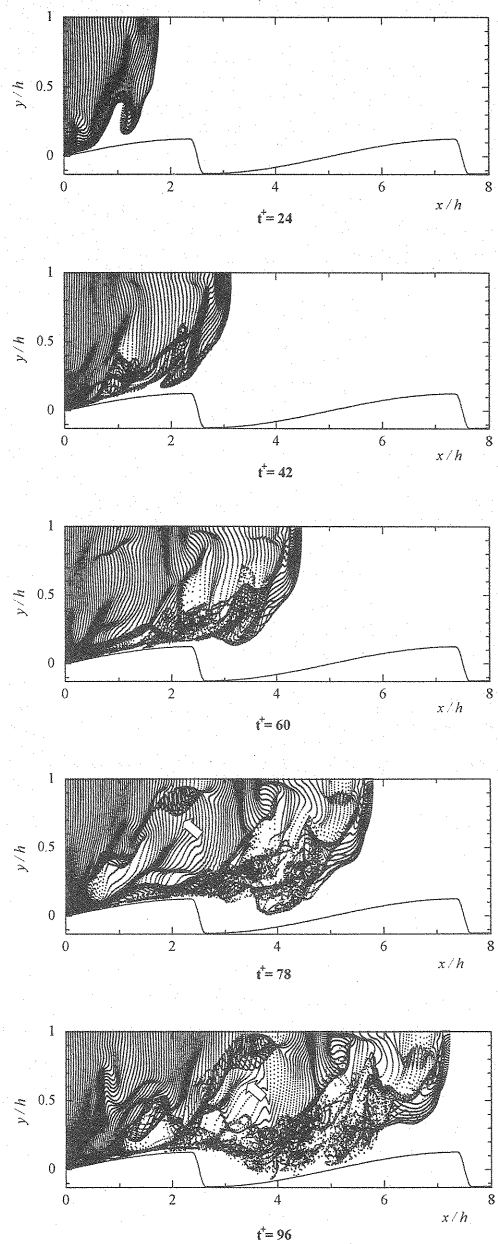

Fig. 6 Time-line diagrams for a vertical plane (z/h=1.25)

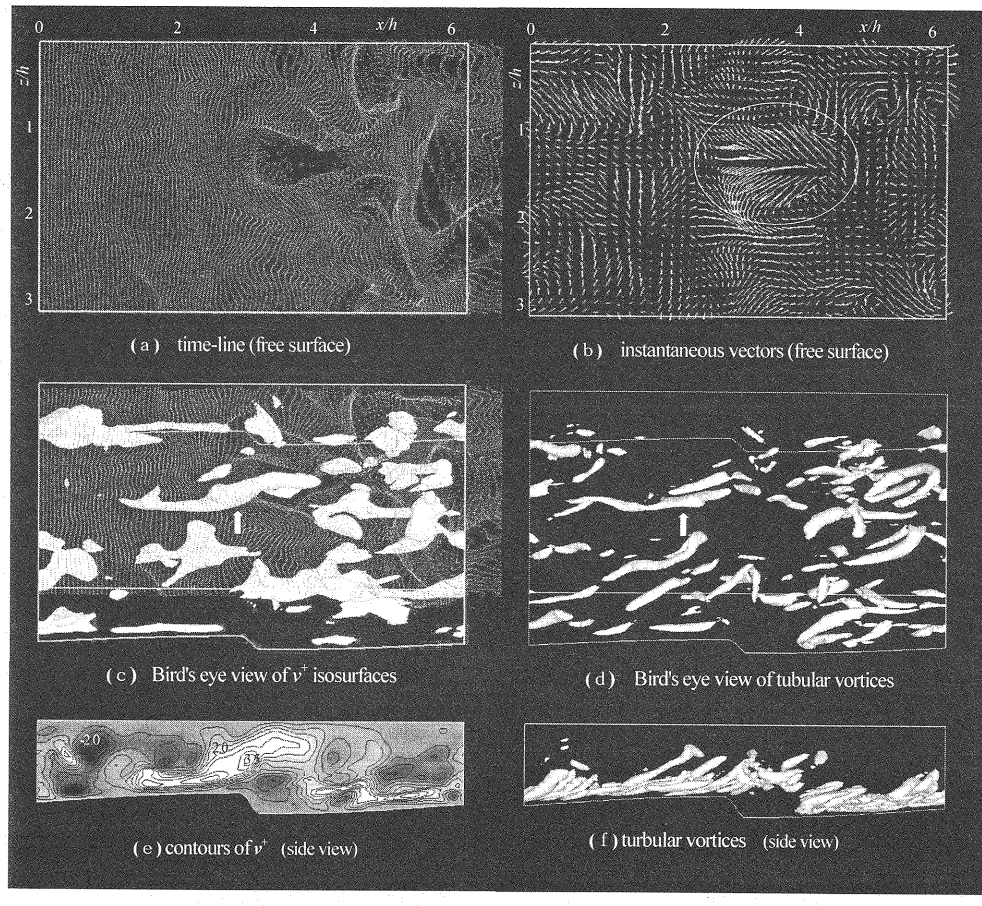

Fig. 7 Visualized coherent vortex structures over a dune-type bed

For $t^+ = 95$, Figure 7 shows: (a) a time-line diagram ($y/h = 0.95$), (b) instantaneous velocity vectors ($y/h = 0.95$), (c) v^+ isosurfaces ($v^+ = 2.0$), (d) coherent structures by the Q definition method , (e) v^+ contours ($z/h = 1.25$) and (f) a side view of tubular vortices. It is evident from (a), (c) and (e) that the boil is caused by a kolk vortex involving a strong upwelling current arising from the riverbed. That the kolk is a rotating tubular vortex is shown by (d) and (e). The instantaneous surface vectors in (b) show an elliptical area extending downstream with no indication of rotational components.

The flow field around the kolk vortex was further investigated in detail. Figure 8 shows instantaneous vectors viewed from upstream on y-z cross sections near the kolk vortex indicated by the arrow in Figure 7(d). Figure 9 shows instantaneous vectors on x-z horizontal planes. Both figures indicate the presence of a strong rotational current around the kolk vortex. While the rotational current rapidly attenuates in the downstream side of the kolk vortex, a counter clockwise compensating vortex occurs so that a pair of vortices which have opposite rotational directions swirl up to the surface causing a boil. As a result, the boil observed on the surface has an elliptical shape extending downstream. The kolk vortex rotates counter clockwise, facing downstream, and is tilted to the right side, although the tilt is not so outstanding as the coherent structures over longitudinal ridges [5]. The kolk vortex is therefore a cyclonic vortex [9] that is tilted so that the sign of the spanwise component of vorticity is the same as the sign of the mean flow vorticity.

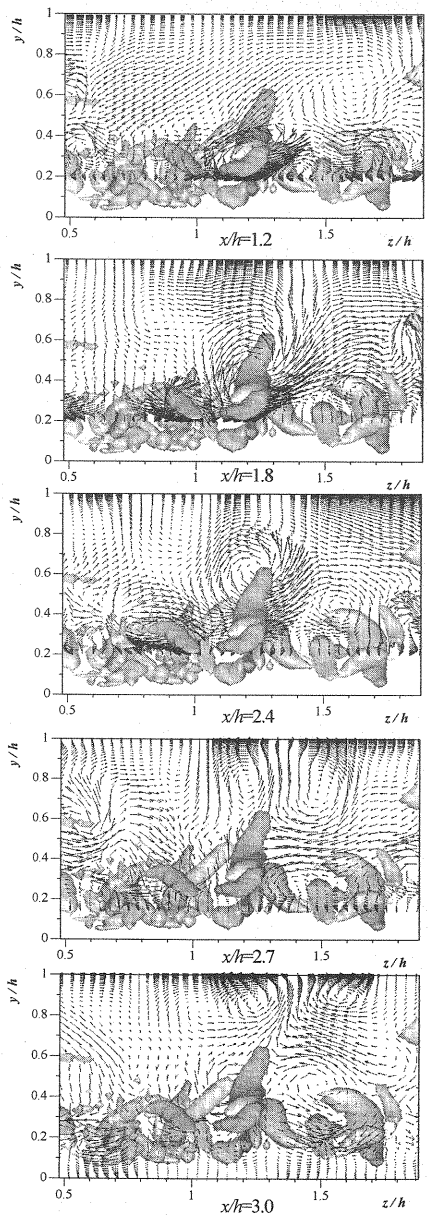

Fig. 8 Instantaneous vectors around a kolk vortex (*y*-*z* plane)

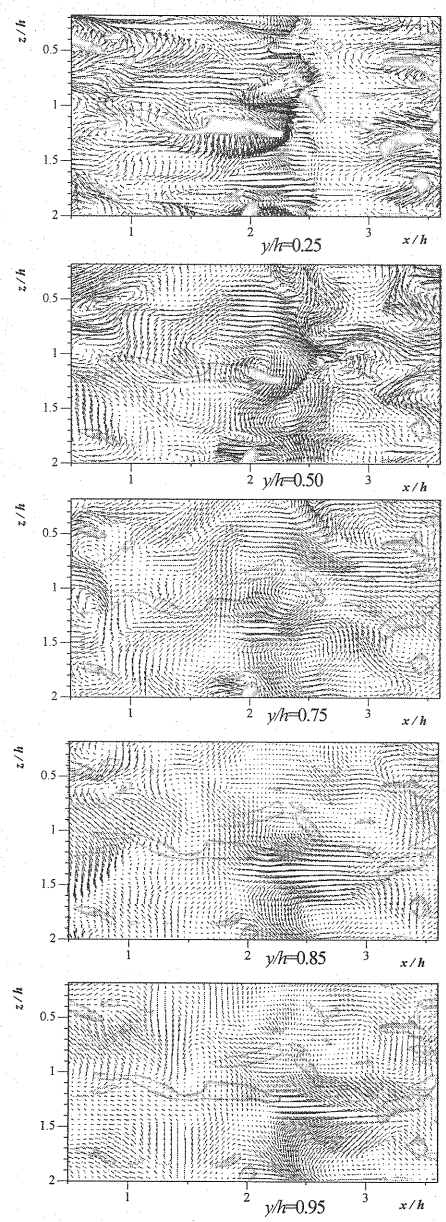

Fig. 9 Instantaneous vectors around a kolk vortex (*x*-*z* plane)

GENERATION CONFIGURATION OF KOLK-BOIL VORTICES

As shown in Figure 7(f), coherent structures above the dune-type riverbed occur downstream from the reattachment point. In this numerical simulation, frequent generations of hairpin vortices were observed. While a hairpin vortex

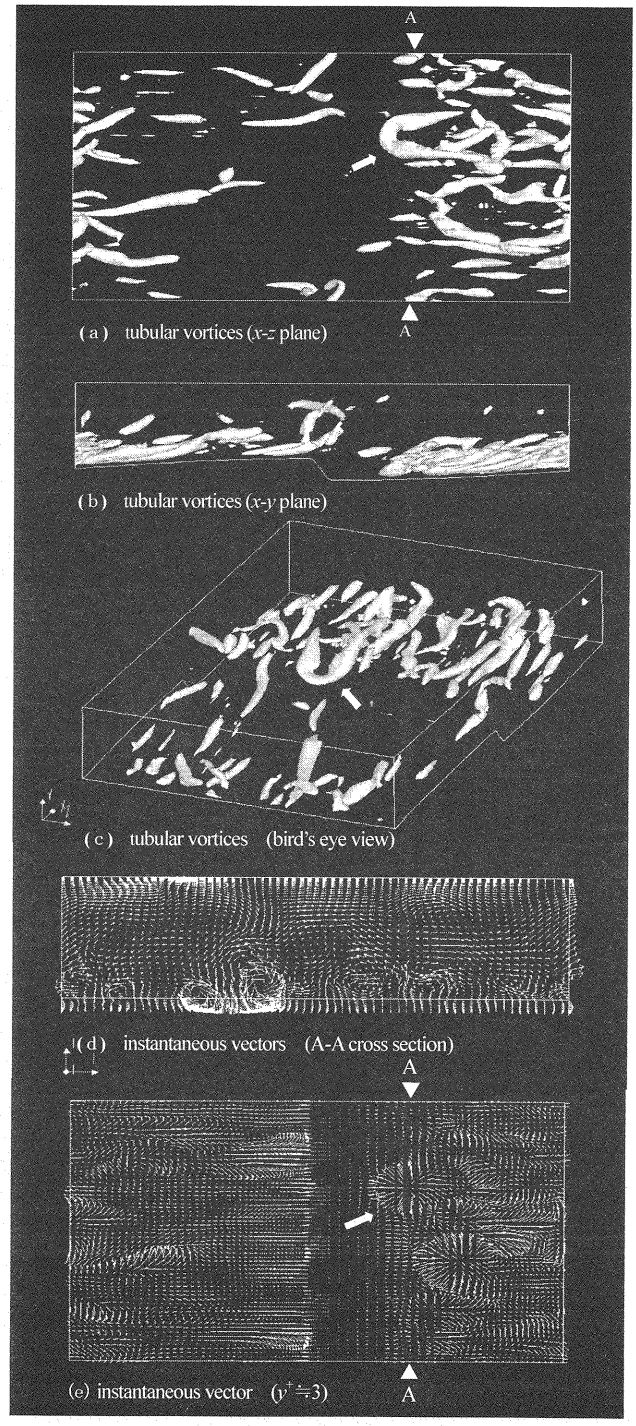

Fig. 10 Views of a reverse hairpin vortex

model has explained boils, kolk-boil vortices may have structures different from the model because the former model cannot explain boils aligned in the spanwise direction. When animated tubular vortices were observed over a long time span, the presence of another characteristic coherent structure, shown by white arrows in Figure 10(a) (c) (e), was recognized. This structure resembles a hairpin vortex from the view point of its shape and tilt angle, but it is actually a U-shaped "reverse hairpin vortex" with its head near the bed and open legs closer to the free surface. Figure 10(d) shows instantaneous vectors in a *y-z* cross-section along the A-A line, which passes the legs of the reverse hairpin vortex. This vortex consists of a pair of cyclonic vortices, while the right-side leg (viewed from upstream) is a counter clockwise vortex extending to the upper right and the left-side leg is a clockwise vortex extending to the upper left. The kolk vortex identified in the previous chapter was traced back, and its origin was found to be the right-side leg of a reverse hairpin vortex. Although not confirmed by computation in this study, two boils aligned in the span direction can be explained by the evolution of both legs of a reverse hairpin vortex into kolk vortices. No evidence of evolution of hairpin vortices into boils was found while making the observations throughout this study. The above findings indicate that boils of the first kind and their causal kolk vortices are generated not only from hairpin vortices but also from reverse hairpin vortices.

CONCLUSIONS

Flow fields on a continuous fixed wavy surface simulating dune-type sand waves were reproduced by DNS and coherent structures were investigated through time-line analyses and visualization of tubular vortices. The following findings were obtained:

(1) DNS was applied to flow fields over dune-type sand waves. Existing experimental results, including mean flow characteristics, reattachment point, and boils characteristic of such flow fields, were reproduced.

(2) Kolk vortices, which can be identified as tubular vortices arising from the riverbed, are characterized by rapid attenuation of rotation and induction of compensating vortices near the free surface. This interaction is reflected in the elliptical shape of boil extending downstream on the free surface.

(3) Boils of the first kind and their causal kolk vortices are generated from "reverse hairpin vortices," whose head is near the bed and cyclonic vortices at their legs.

REFERENCES

1. Daiguji,H.,Miyake,Y.and Yoshizawa,A. ed. : Computational Fluid Dynamics of Turbulent Flow - Models and Numerical Methods, Univ.Tokyo press,1998. (in Japanese)
2. Hayashi,S., Ohmoto,T, Yakita,K., and Hirakawa,R. : Direct numerical simulation of turbulent flow using high-order accuracy upwind difference scheme, Proceedings of the 12th Congress of The Asia and Pacific Division International Association of Hydraulic Engineering and Research, Bangkok, Thailand, pp.65-75, 2000.
3. Hayashi,S. and Ohmoto,T. : Direct numerical simulation of open-channel turbulent flow using a regular grid in a generalized coordinate system, Journal of Hydroscience and Hydraulic Engineering, Japan Society of Civil Engineering , Vol.19, No.1, pp. 65-74, 2001.
4. Hayashi,S.,Ohmoto,T. and Takikawa,K. : Fundamental study on direct numerical simulation using a high-order accuracy upwind difference scheme, Journal of Hydroscience and Hydraulic engineering, Japan Society of Civil Engineering , Vol.19, No.2, pp.93-104, 2001.
5. Hayashi,S.,Ohmoto,T. and Takikawa,K. : Study on three-dimensional turbulent shear flow structure over sand ridges by direct numerical Simulation, Journal of Applied Mechanics, Japan Society of Civil Engineering, Vol.4, pp.591-600, 201. (in Japanese)
6. Hunt,J.C.R., Wray,A.A. and Moin,P. : Eddies, stream, and convergence zones in turbulent flows, Center for Turbulence Research Report CTR-S88, 1988.
7. Jackson,R.G. : Sedimentological and fluid-dynamic implications of the turbulent bursting phenomenon in geophysical flows, Journal of Fluid Mech., Vol.77, pp. 531-560, 1976.
8. Jeong,J. and Hussain,F. : On the identification of a vortex, Journal of Fluid Mech., Vol.285, pp.69-94, 1995.

9. Kida,S. and Tanaka,M. : Dynamics of vortical structures in a homogeneous shear flow. Journal of Fluid Mech., Vol.239, pp. 43-68, 1994.
10. Matthes,G.H. : Macroturbulence in natural stream flow, Amer.Geophy.Union, Vol.28, pp.255-265, 1947.
11. Nezu,I. and Nakagawa.,H. : Turbulence in Open- Channel Flows, IAHR - Monograph, Balkema, 1993.
12. Nezu,I. and Nakagawa,H. : Three-dimensional structures of coherent vortices generated behind dunes in turbulent free-surface flows, Refind Flows Modelling and Turbulence Measurements, Proc.of the 5thIint.symp., pp.603-612, 1993.
13. Nezu,I., Kadota,A. and Kurata,M. : Free-surface flow structure of space-time correlation of coherent vortices generated behind dune bed, Proc.of the 6th Int. Symp. on flow modeling and turbulence measurements, pp.695-701, 1996.
14. Nezu,I., Kadota,A., Shinbashi,H. and Kurata,M. : The structures of space-time correlations in unsteady open-channel flow over dunes, Journal of Hydraulic Coastal and Environmental Engineering, Japan Society of Civil Engineering , No.579／II-41, pp.125-136, 1997.11.
15. Nezu,I., Kadota,A. and He, J. : Numerical simulation on turbulent structures in open-channel flows over dunes, Journal of Hydraulic Engineering, Japan Society of Civil Engineering , Vol.41, pp. 669-674, 1997. (in Japanese)
16. Steger,J.L. and Sorenson,R.L. : Automatic mesh-point clustering near a boundary in grid generation with elliptic partial differential equations, Journal of Computational Phys. 33. pp.405-410. 1979.

APPENDIX – NOTATION

The following symbols are used in this paper :

h	= flow depth ;
p	= pressure ;
Q	= the second invariant ;
Re	= Reynolds number ;
s_{ij}	= instantaneous velocity-gradient tensor ;
S_{ij}	= mean velocity-gradient tensor ;
t	= time ;
u_*	= friction velocity ;
u,v,w	= instantaneous velocities in the x , y and z direction ;
$-\overline{u^+v^+}$	= Reynolds stress
U,V,W	= mean velocities in the x , y and z direction ;
x,y,z	= coordinates of streamwise,vertical and spanwise direction ;
Δt	= time increment ;
Δx , Δy , Δz	= spatial increment in the x , y and z direction ;
$\Delta x^+, \Delta y^+, \Delta z^+$	= dimensionless spatial increment in the coordinate x , y and z direction ;
ξ_j	= coordinates in the computational plane ; and
Ω	= vorticity tensor.

The superscript

+	= non-dimensional coordinate normalized by the viscous length.

(Received July 2, 2002 ; revised March 19, 2003)